

# Estimating Meteorological Visibility using Cameras: a Probabilistic Model-Driven Approach

Nicolas Hautière<sup>1</sup>, Raouf Babari<sup>1</sup>, Éric Dumont<sup>1</sup>, Roland Brémond<sup>1</sup>, and Nicolas Paparoditis<sup>2</sup>

<sup>1</sup> Université Paris-Est, LEPSIS, INRETS-LCPC  
58 boulevard Lefebvre, F-75015 Paris

<sup>2</sup> Université Paris-Est, MATIS, IGN  
73 avenue de Paris, F-94160 Saint-Mandé  
nicolas.hautiere@lcpc.fr

**Abstract.** Estimating the atmospheric or meteorological visibility distance is very important for air and ground transport safety, as well as for air quality. However, there is no holistic approach to tackle the problem by camera. Most existing methods are data-driven approaches which perform a linear regression between the contrast in the scene and the visual range estimated by means of reference additional sensors. In this paper, we propose a probabilistic model-based approach which takes into account the distribution of contrasts in the scene. It is robust to illumination variations in the scene by taking into account the Lambertian surfaces. To evaluate our model, meteorological ground truth data were collected, showing very promising results. This work opens new perspectives in the computer vision community dealing with environmental issues.

## 1 Introduction

Estimating the atmospheric or meteorological visibility distance is very important for transport safety and for air quality monitoring. Dedicated optical sensors exist but are very expensive. For this reason, they are deployed only in crucial places like airports. Thus, the use of outdoor cameras is of great interest since they are low cost and already deployed for other purposes like showing current traffic and weather conditions [1].

Some attempts are reported in the literature to estimate the visibility using outdoor cameras or webcams. However, the visibility range differs from one application to another, so that there is no holistic approach to tackle the problem by camera. For road safety applications, the range 0-400 m is usually considered. For meteorological observation and airport safety, the range 0-1000 m is usually considered. Visual range is also used for monitoring pollution in urban areas. In this case, higher visual ranges, typically 1-5 km, are usually considered. In this paper, we propose a method which copes with the different application constraints.

Two families of methods are proposed in the literature. The first one estimates the maximum distance at which a selected target can be seen. The methods differ depending on the nature of the target and how to estimate the distance. For intelligent vehicles as well as for visual monitoring of highway traffic, a black target at the horizon is chosen and a flat road is assumed. Bush [2] uses a wavelet transform to detect the

highest edge in the image with a contrast above 5%. Based on a highway meteorology standard, Hautière et al. [3] proposed a reference-free roadside camera-based sensor which not only estimates the visibility range but also detects that the visibility reduction is caused by fog. For meteorological observations, regions of interest whose distance can be obtained on standard geographic maps are selected manually [4]. An accurate geometric calibration of the camera is necessary to operate these methods.

A second family of methods correlates the contrast in the scene with the visual range estimated by reference additional sensors [5]. No accurate geometric calibration is necessary. Conversely, a learning phase is needed to estimate the function which maps the contrast in the scene to the visual range. The method proposed in this paper belongs to this second family. Usually, a simple gradient based on the Sobel filter or a high-pass filter in the frequency domain are used to compute the contrast [6–8]. Luo et al. [9] have shown that the visual range obtained with both approaches are highly correlated. Liaw et al. [6] proposed to use a homomorphic filter in addition to the high-pass filter in order to reduce the effects of non-uniform illumination. Once the contrast is computed, a linear regression is performed to estimate the mapping function [5, 8, 6]. Due to this step of linear regression, these methods can be seen as data driven approaches.

Unlike previous data-driven approaches, we propose a probabilistic model-driven approach which allows computing a physics-based mapping function. Unlike existing approaches, our model is non-linear, which allows encompassing the whole spectrum of applications. In particular, our model takes into account the distribution of contrasts in the scene. Unlike existing approaches, e.g. [8], our model is robust to illumination variations in the scene by taking into account the physical properties of objects in the scene. To assess the relevance of our approach, we have collected ground truth data. Using these rare experimental data, we are able to present very promising results, which might open new trends in the computer vision community dealing with environmental issues.

The remainder of this paper is organized as following. In section 2, we recall the Koschmieder’s model of fog visual effects on which we base our work. In section 3, we present a model-driven approach, whose experimental evaluation is carried out in section 4. Finally, we discuss the results and conclude.

## 2 Vision through the Atmosphere

The attenuation of luminance through the atmosphere was studied by Koschmieder [10], who derived an equation relating the extinction coefficient of the atmosphere  $\beta$ , the apparent luminance  $L$  of an object located at distance  $d$ , and the luminance  $L_0$  measured close to this object:

$$L = L_0 e^{-\beta d} + L_\infty (1 - e^{-\beta d}) \quad (1)$$

(1) indicates that the luminance of the object seen through fog is attenuated by  $e^{-\beta d}$  (Beer-Lambert law); it also reveals a luminance reinforcement of the form  $L_\infty (1 - e^{-\beta d})$  resulting from daylight scattered by the slab of fog between the object and the observer, the so-called airlight.  $L_\infty$  is the atmospheric luminance.

On the basis of this equation, Duntley developed a contrast attenuation law [10], stating that a nearby object exhibiting contrast  $C_0$  with the fog in the background will

be perceived at distance  $d$  with the following contrast:

$$C = \left[ \frac{L_0 - L_\infty}{L_\infty} \right] e^{-\beta d} = C_0 e^{-\beta d} \quad (2)$$

This expression serves to base the definition of a standard dimension called meteorological visibility distance  $V$ , i.e. the greatest distance at which a black object ( $C_0 = -1$ ) of a suitable dimension can be seen on the horizon, with the threshold contrast set at 5% [11]. It is thus a standard parameter that characterizes the opacity of a fog layer. This definition yields the following expression:

$$V \approx \frac{3}{\beta} \quad (3)$$

More recently, Koschmieder's model has received a lot of attention in the computer vision community, e.g. [12–17]. Indeed, thanks to this model, it is possible to infer the 3D structure of a scene in fog presence, or to dehaze/defog images by reversing the model. However, it is worth mentioning that in these works a relative estimation of the meteorological visibility is enough to restore the visibility. In this paper, we use Koschmieder's model to estimate the actual meteorological visibility distance, which makes the problem quite different.

### 3 The Model-Driven Approach

#### 3.1 Contrast of a Distant Target

Assuming a linear response function of the camera, the intensity  $I$  of a distant point located at distance  $d$  in an outdoor scene is given by Koschmieder's model (1):

$$I = R e^{-\beta d} + A_\infty (1 - e^{-\beta d}) \quad (4)$$

where  $R$  is the intrinsic intensity of the pixel, i.e. the intensity corresponding to the intrinsic luminance value of the corresponding scene point and  $A_\infty$  is the background sky intensity. Two points located at roughly the same distance  $d_1 \approx d_2 = d$  with different intensities  $I_1 \neq I_2$  form a distant target whose normalized contrast is given by:

$$C = \frac{I_2 - I_1}{A_\infty} = \left[ \frac{R_2 - R_1}{A_\infty} \right] e^{-\beta d} = C_0 e^{-\beta d} \quad (5)$$

In this equation, the contrast  $C$  of a target located at  $d$  depends on  $V = \frac{3}{\beta}$  and on its intrinsic contrast  $C_0$ . If we now assume that the surface of the target is Lambertian, the luminance  $L$  at each point  $i$  of the target is given by:

$$L = \rho_i \frac{E}{\pi} \quad (6)$$

where  $\rho_i$  denotes the albedo at  $i$ . Moreover, it is a classical assumption to set  $L_\infty = E/\pi$  so that (5) finally becomes:

$$C = (\rho_2 - \rho_1) e^{-\beta d} \approx (\rho_2 - \rho_1) e^{-\frac{3d}{V}} = \Delta\rho \times e^{-\frac{3d}{V}} \quad (7)$$

Consequently, the contrast of a distant Lambertian target only depends on its physical properties and on its distance to the sensor and on the meteorological visibility distance, and no longer on the illumination. These surfaces are robust to strong illumination variations in the computation of the contrast in the scene.

### 3.2 Probabilistic Modeling

Let us consider an outdoor scene where targets are distributed at different distances from the camera. Let us denote  $\phi$  the probability density function of observing a contrast  $C$  in the scene:

$$\mathbb{P}(C < X \leq C + dC) = \phi(C)dC \quad (8)$$

We denote  $\psi$  the p.d.f. of there being a target at the distance  $d$ . Thanks to (7),  $\phi$  can be written as a function of  $\psi$ :

$$\phi(C) = -\frac{V}{3C\Delta\rho} \psi(d) \quad (9)$$

The mean contrast in the scene can thus be computed thanks to the density of targets in the scene:

$$m = \int_0^1 C\phi(C)dC = \int_0^{+\infty} \Delta\rho\psi(d)e^{-\frac{3d}{V}} dd \quad (10)$$

To express  $m$ , a realistic expression for the density of targets  $\psi$  in the scene is needed.

### 3.3 Expectation of the Mean Contrast

In this paragraph, we search an analytical expression of (10). In this aim, we assume a scene which contains  $n$  Lambertian targets with random albedos located at random distances between 0 and  $d_{\max}$ . For a given sample scene, we can compute the mean contrast of the targets with respect to the meteorological visibility distance and plot the corresponding curve. Some sample curves are plotted in blue in Fig. 1 ( $n = 100$  and  $d_{\max} = 1000$  m). We can compute the mathematical expectation of the mean contrast and obtain the following analytical model:

$$m_u = \frac{V\Delta\bar{\rho}}{6d_{\max}} \left[ 1 - \exp\left(-\frac{3d_{\max}}{V}\right) \right] \quad (11)$$

where  $\Delta\bar{\rho}$  is the mean albedo difference of the targets in the scene. We plot this model in red in Fig. 1. If we do not have any a priori on the targets distribution in the scene, this analytical model is the most probable with which to fit the data. That will be experimentally assessed in section 4.

At this stage, we can make a comparison with the charging/discharging of a capacitor. The capacitance of the system is determined by the distribution of Lambertian targets in the scene. The smaller the capacitance of the system is, the faster the curves go to 0.5. We thus define an indicator  $\tau$  of the system quality which is the meteorological visibility distance at which two thirds of the "capacitance" is reached. A high value of  $\tau$  also means a lower sensitivity of the model at low meteorological visibility distances.

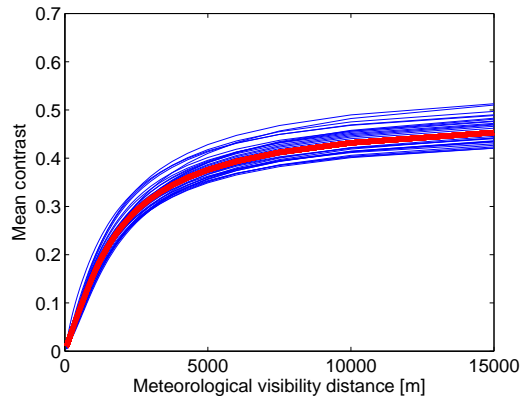


**Fig. 1.** Blue: curves depicting the mean contrast in random scenes with respect to the meteorological visibility distance. Red: expectation of the mean contrast.

### 3.4 Model Inversion and Error Estimation

In the previous section, we have computed an analytical expression of the mean contrast expectation  $m_u$  with respect to the meteorological visibility distance  $V$ . Ultimately, we would like to compute  $V$  as a function of  $m_u$ . In this aim, we need to invert the mean contrast expectation function (11). The inversion of this model exists and is expressed by:

$$V(m_u) = \frac{3m_u d_{\max}}{1 + m_u W\left(\frac{e^{-1/m_u}}{m_u}\right)} \quad (12)$$

where Lambert  $W$  is a transcendental function defined by solutions of the equation  $We^W = x$  [18].

## 4 Experimental Evaluation

In this section, we present an experimental evaluation of the proposed model for visibility estimation. In this aim, we have collected ground truth data. First, we present the methodology. Second, we present our method to estimate whether a surface is Lambertian or not. Third, we present the results.

### 4.1 Methodology

**Instrumentation.** The observation field test we used is equipped with a reference transmissometer (Degreane Horizon TI8510). It serves to calibrate different scatterometers (Degreane Horizon DF320) used to monitor the meteorological visibility distance on the French territory, one of which provided our data. They are coupled with a background luminance sensor (Degreane Horizon LU320) which monitors the illumination

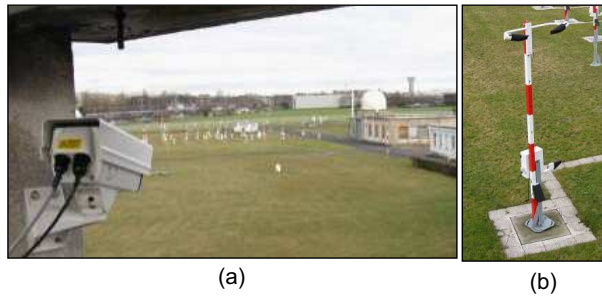


**Fig. 2.** Instrumentation of our observation field test: (a) the camera grabbing pictures of the field test; (b) the scatterometer along with the background luminancemeter.

received by the sensor. We have added a camera which grabs images of the field test every ten minutes. The camera is an 8-bit CCD camera ( $640 \times 480$  definition,  $H=8.3$  m,  $\theta = 9.8^\circ$ ,  $f_l = 4$  mm and  $t_{pix} = 9 \mu m$ ). It is thus a low cost camera which is representative of common video surveillance cameras. Fig. 2(a) shows the installed camera and its orientation with respect to the field test. Fig. 2(b) shows the scatterometer and the background luminancemeter.

**Data collection.** We have collected two fog events at the end of February 2009. The fog occurred early in the morning and lasted a few hours after sunrise. During the same days, there were strong sunny weather periods. Fig. 3 shows sample images. Figs. 3(a) is a sample of sunny weather. Fig. 3(b) is a sample of cloudy weather. Fig. 3(c) is a sample of foggy weather. The corresponding meteorological visibility distances and luminances are plotted in Fig. 3(d,e). As one can see, the meteorological visibility distance ranges from 100 m to 35.000 m and the luminance ranges from 0 to  $6.000 \text{ cd.m}^{-2}$ .

We have thus collected quite rare experimental data. Indeed, during a short period of time, we had rapidly changing weather conditions. The ranges of meteorological visibility distance and luminance were very large. In the literature, works are dedicated to limited ranges of visibility distances. For example, road safety applications are dealing with 0-400 m whereas people working on environmental issues are dealing with meteorological visibility distances which are above 1000 m. We are among the first to have collected data encompassing both ranges. Moreover, since the data were collected in a short period of time, we can consider that the content of the scene did not change. For example, we can consider that the phenology of the trees did not change, so that the amount of texture in the scene without fog remains constant. This database is available on LCPC's web site <http://www.lcpc.fr/en/produits/matilda/> for research purpose.

#### 4.2 Location of Lambertian surfaces.

To estimate  $m$  and thus  $V$ , we compute the normalized gradient only on the Lambertian surfaces of the scene as proposed in section 3.1. We thus need to locate Lambertian

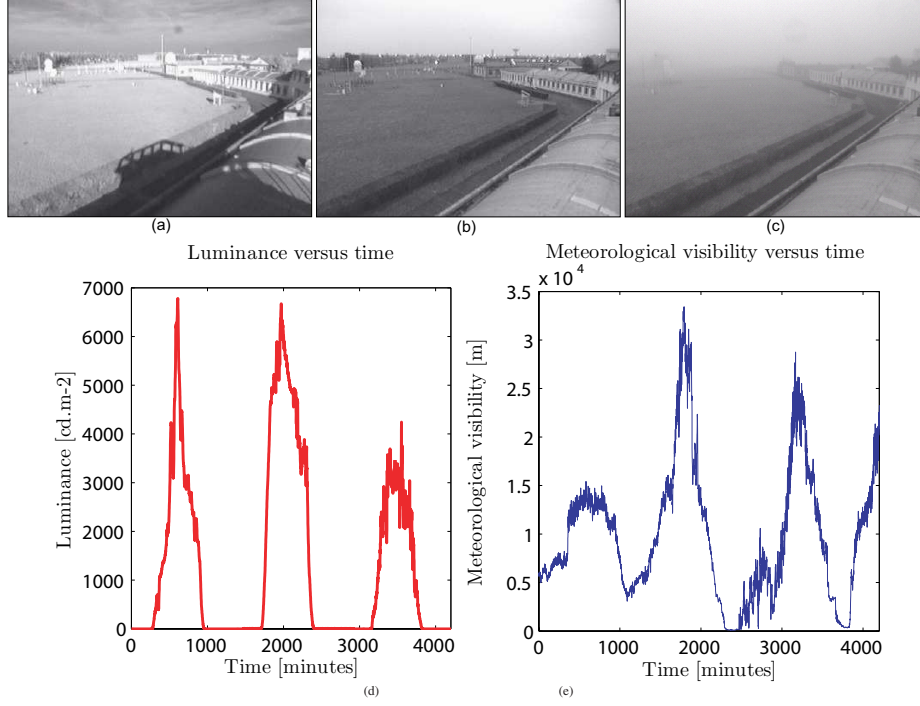


**Fig. 3.** Samples of data collected in winter 2008-2009: (a) images with strong illumination conditions and presence of shadows; (b) cloudy conditions; (c) foggy weather situation; (d) meteorological visibility distance data and (e) background luminance data collected in the field test during two days.

surfaces in the images. In this aim, we compute the Pearson coefficient, denoted  $P_{i,j}^L$ , between the intensity of pixels in image series where the position of the sun changes and the value of the background luminance estimated by the luminancemeter. The closer  $P_{i,j}^L$  is to 1, the stronger the probability that the pixel belongs to a Lambertian surface. This technique provides an efficient way to locate the Lambertian surfaces in the scene. For our field test, the mask of Lambertian surfaces is shown in Fig.4. The redder the pixel, the more the surface is assumed to be Lambertian.

Having located the Lambertian surfaces, we can compute the gradients in the scene by means of the module of the Sobel filter. For each pixel, we normalize the gradient  $G_{i,j}$  by the intensity of the background. Since our camera is equipped with an auto-iris, the background intensity  $A_\infty$  is most of the time equal to  $2^8 - 1$ , so that this step can be avoided. Each gradient is then weighted by  $P_{i,j}^L$ , the probability of a pixel to belong to a Lambertian surface where no depth discontinuity exists ( $P^L$  is mostly very small). Consequently, only relevant areas of the image are used, and the scene need not be



**Fig. 4.** Mask of Lambertian surfaces on our field test: The redder the pixel is, the higher the confidence that the surface is Lambertian.

totally Lambertian. Finally, the estimated contrast in the scene  $\tilde{m}_u$  is given by:

$$\tilde{m}_u = \sum_{i=0}^H \sum_{j=0}^W \Delta\rho_{i,j} \exp\left(-\frac{3d_{i,j}}{V}\right) \approx \sum_{i=0}^H \sum_{j=0}^W \frac{G_{i,j}}{A_\infty} P_{i,j}^L \quad (13)$$

where  $\Delta\rho_{i,j}$  is the intrinsic contrast of a pixel (7), and  $H$  and  $W$  are respectively the height and the width of the images. Finally, the approach makes the best use of the physics of the scene and would be able to process scenes without any Lambertian surfaces (at the cost of lowering the quality of the results).

### 4.3 Results

**Contrast estimators.** We have computed (13) for our collection of 150 images with different meteorological visibility distances. For comparison purposes, we have also computed the simple sum of gradients in the image without taking into account the segmentation of the Lambertian surfaces. The results are shown in Fig. 5. Using the Lambertian surfaces, we can see that the shape of the distribution in Fig. 5(a) looks like the curve proposed in Fig. 1, which is very satisfactory. Conversely, when all the pixels of the scene are used, the points are more scattered when the meteorological visibility distance is above 2500 m (see Fig. 5(b)). When the visibility is above 2500 m, the illumination by the sun does influence a lot the gradients in the scene. When the weather is sunny, i.e. the visibility is better, the influence of the sun is more important so that the gradient is changing with respect to the sun position. Consequently, the estimation of the visibility is altered. These two distributions show the benefit of selecting the Lambertian surfaces to estimate the visibility distance.

**Model fitting.** We have to fit the mean contrast model (11) to the data shown in Fig. 5(a) using robust regression techniques. To ensure a mathematical solution, we have fitted the model (14), which is slightly different from the theoretical model. Three unknown

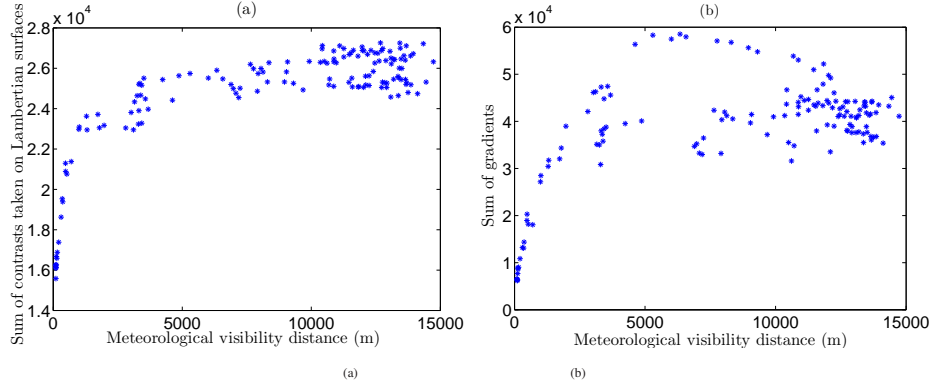


**Fig. 5.** Visibility estimators: (a) the estimator is based on the contrast on Lambertian surfaces; (b) the estimator is only based on Sobel’s gradient module.

variables  $a$ ,  $b$  and  $d_{max}$  have to be estimated, which can be easily done using classical curve fitting tools.

$$\tilde{m}_u = \frac{aV}{d_{max}} \left[ 1 - \exp\left(-\frac{3d_{max}}{V}\right) \right] + b \quad (14)$$

This model fits well with the data ( $R^2 = 0.91$ ). In particular, we obtain  $d_{max} = 307.2$  m. The fitted curve is plotted in Fig. 6. We estimated a capacitance of the system  $\tau \approx 950$  m.

**Discussions.** From the fitted model, we can now invert the model using (12) and estimate the meteorological visibility distance  $\tilde{V}$  based on the mean contrast  $m_u$ :

$$\tilde{V} = \frac{3d_{max}(b - m_u)}{(b - m_u)W\left(\frac{ae^{\frac{a}{b - m_u}}}{b - m_u}\right) - a} \quad (15)$$

Having estimated the meteorological visibility distance, we can compute the error on this estimation. The results are given in Tab. 1. Since the applications are very different depending on the range of meteorological visibility distances, we have computed the error and the standard deviation for various applications: road safety, meteorological observation and air quality. One can see that the error remains low for critical safety applications. It increases for higher ranges of visibility distances, and becomes huge for visibility distances above 7 km.

Different points may be discussed. First, the model used in this paper is relevant for uniform distribution of distances which happen in many environments, such as highway scenes. The scene from which the experimental data used in this paper are issued may be not meet this assumption. Second, the Sobel operator is certainly not the best estimate for the gradient. Indeed, it is a simple high-pass filter which is problematic because of the impulse noise of camera sensors. Different filters may be used to beforehand enhance the images, or to compute the contrast more robustly.

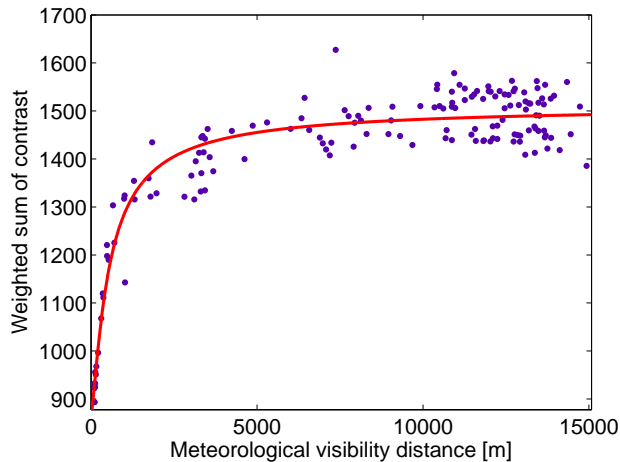


Fig. 6. Data fitting with the mean contrast model. Dots: data. Red curve: fitted model.

Application	Highway fog	Meteorological fog	Haze	Air quality
Range [m]	0-400	0-1000	0-5000	0-15000
Number of data	13	19	45	150
Mean error [%]	12.6	18.1	29.7	-
Std [%]	13.7	18.9	22	-

Table 1. Relative errors of meteorological visibility distance estimation with respect to the envisaged application.

## 5 Conclusion

In this paper, we propose a probabilistic model-driven approach to estimate the meteorological visibility distance through use of generic outdoor cameras based on a mean contrast expectation function. Unlike previous data-driven approaches, we use a physical model which allows computing a mapping function between the contrast and the meteorological visibility estimated by an additional reference sensor. Our model is non-linear which allows dealing with a large spectrum of applications. The calibration of our system is less sensitive to the input data due to its intrinsic physical constraints. In particular, our model takes into account the distribution of targets in the scene. It is also robust to illumination variations in the scene by taking into account the Lambertian surfaces. To evaluate the relevance of our approach, we have collected ground truth data with the help of our national meteorological institute. Using these rare experimental data, we obtain promising results. In future work, we intend to estimate the contrast expectation function without any additional meteorological sensor, based only on the properties of the scene (geometry, texture) collected by remote sensing techniques and the characteristics of the camera. Such a model-driven approach paves the road to methods without any learning phases.

## References

1. Jacobs, N., W., B., Fridrich, N., Abrams, A., Miskell, K., Brswell, B., Richardson, A., Pless, R.: The global network of outdoor webcams: Properties and applications. In: ACM International Conference on Advances in Geographic Information Systems (ACM GIS'09). (2009)
2. Bush, C., Debes, E.: Wavelet transform for analyzing fog visibility. *IEEE Intelligent Systems* **13**(6) (November/December 1998) 66–71
3. Hautière, N., Bigorgne, E., Bossu, J., Aubert, D.: Meteorological conditions processing for vision-based traffic monitoring. In: International Workshop on Visual Surveillance, European Conference on Computer Vision. (2008)
4. Bäumer, D., Versick, S., Vogel, B.: Determination of the visibility using a digital panorama camera. *Atmospheric Environment* **42** (2008) 2593–2602
5. Hallowell, R., Matthews, M., Pisano, P.: An automated visibility detection algorithm utilizing camera imagery. In: 23rd Conference on Interactive Information and Processing Systems for Meteorology, Oceanography, and Hydrology (IIPS), San Antonio, TX, Amer. Meteor. Soc. (2007)
6. Liaw, J.J., Lian, S.B., Chen, R.C.: Atmospheric visibility monitoring using digital image analysis techniques. In Jiang, X., Petkov, N., eds.: International Conference on Computer Analysis of Images and Patterns. Volume 5702 of LNCS. (2009) 1204–1211
7. Hagiwara, T., Ota, Y., Kaneda, Y., Nagata, Y., Araki, K.: A method of processing CCTV digital images for poor visibility identification. *Transportation Research Records* **1973** (2007) 95–104
8. Xie, L., Chiu, A., Newsam, S.: Estimating atmospheric visibility using general-purpose cameras. In Bebis, G., ed.: International Symposium on Visual Computing, Part II. Volume 5359 of LNCS. (2008) 356–367
9. Luo, C.H., Wen, C.Y., Yuan, C.S., Liaw, J.-L. and Lo, C.C., Chiu, S.H.: Investigation of urban atmospheric visibility by high-frequency extraction: Model development and field test. *Atmospheric Environment* **39** (2005) 2545–2552
10. Middleton, W.: Vision through the atmosphere. University of Toronto Press (1952)
11. CIE: International Lighting Vocabulary. Number 17.4. (1987)
12. Narasimhan, S.G., Nayar, S.K.: Vision and the atmosphere. *Int J Comput Vis* **48**(3) (2002) 233–254
13. Narasimhan, S.G., Nayar, S.K.: Contrast restoration of weather degraded images. *IEEE Transactions on Pattern Analysis and Machine Intelligence* **25**(6) (June 2003) 713–724
14. Hautière, N., Tarel, J.P., Aubert, D.: Towards fog-free in-vehicle vision systems through contrast restoration. In: IEEE Conference on Computer Vision and Pattern Recognition, Minneapolis, Minnesota, USA. (2007)
15. Tan, R.T.: Visibility in bad weather from a single image. In: IEEE Conference on Computer Vision and Pattern Recognition, Anchorage, Alaska, USA. (2008)
16. He, K., Sun, J., Tang, X.: Single image haze removal using dark channel prior. In: IEEE Conference on Computer Vision and Pattern Recognition, Miami, Florida, USA. (2009)
17. Tarel, J.P., Hautière, N.: Fast visibility restoration from a single color or gray level image. In: IEEE International Conference on Computer Vision, Kyoto, Japan. (2009)
18. Corless, R.M., Gonnet, G.H., Hare, D.E.G., Jeffrey, D.J., Knuth, D.E.: On the Lambert W function. *Advances in Computational Mathematics* **5** (1996) 329–359